

Bathymetric Influence on the Coastal Sea Level Response to Ocean Gyres at Western Boundaries

ANTHONY WISE

National Oceanography Centre, and Department of Earth and Ocean Sciences, University of Liverpool, Liverpool, United Kingdom

CHRIS W. HUGHES

Department of Earth and Ocean Sciences, University of Liverpool, and National Oceanography Centre, Liverpool, United Kingdom

JEFF A. POLTON

National Oceanography Centre, Liverpool, United Kingdom

(Manuscript received 22 January 2018, in final form 22 September 2018)


ABSTRACT

It is our aim with this paper to investigate how the presence of a continental shelf and slope alters the relationship between interior ocean dynamics and western boundary (coastal) sea level. The assumption of a flat-bottomed basin with vertical sidewall at the coast is shown to hide the role that depth plays in the net force acting on the coast. A linear β -plane theory is then developed describing the transmission of sea level over variable depth bathymetry as analogous to the steady advection–diffusion of a thermal fluid. The parameter $P_a = \beta H L^{(s)}/r$, relating the friction parameter r to the bathymetry depth H and width $L^{(s)}$, is found to determine the contribution of interior sea level to coastal sea level, with small P_a giving maximum penetration and large P_a maximum insulation. In the small P_a (infinite friction) limit the frictional boundary layer extends far offshore, and coastal sea level tends toward the vertical sidewall solution. Adding simple stratification produces exactly the same result but with reduced effective depth and hence enhanced penetration. Penetration can be further enhanced by permitting weakly nonlinear variations of thermocline depth. Wider and shallower shelves relative to the overall scales are also shown to maximize penetration for realistic values of P_a (≤ 10). The theory implies that resolution of bathymetry and representation of friction can have a large impact on simulated coastal sea level, calling into question the ability of coarse-resolution models to accurately represent processes determining the dynamic coastal sea level.

1. Introduction

Improvements in geoid determination enabled [Woodworth et al. \(2012\)](#), [Higginson et al. \(2015\)](#), and [Lin et al. \(2015\)](#) to demonstrate that sea level (SL) along coastal boundaries can differ markedly from the adjacent open ocean (interior). In particular, [Higginson et al. \(2015\)](#) showed that between the Florida Keys and Halifax, Canada, the approximately 1-m northward drop in SL across the Gulf Stream is missing at the coast, replaced by a smaller 20-cm drop some 10° farther south.

While SL (specifically ocean surface dynamic topography) gradients in the deep ocean are approximately in geostrophic balance, the zero normal-flow condition imposed by continents implies this balance does not describe coastal alongshore SL gradients. The threat of rising global SL has motivated the investigation of the drivers of coastal SL globally and is of particular interest along the North American east coast owing to the identification of a SL rise “hot spot” ([Sallenger et al. 2012](#)). Advancing our understanding of the basic processes relating coastal to interior SL, particularly where strong western boundary

 Denotes content that is immediately available upon publication as open access.

Corresponding author: Anthony Wise, anwise@noc.ac.uk



This article is licensed under a [Creative Commons Attribution 4.0 license](http://creativecommons.org/licenses/by/4.0/) (<http://creativecommons.org/licenses/by/4.0/>).

currents and complex bathymetry are present, is fundamental to building confidence in the predictions of numerical models.

For basins modeled with flat bottoms and vertical sidewalls, [Stommel \(1948\)](#) showed that a solution for the circulation could be found by balancing the vorticity added by wind stress with bottom friction. This approach resulted in boundary layers running north–south, which [Munk \(1950\)](#) further developed by replacing bottom friction with lateral friction, a more realistic assumption for flows that do not reach the bottom. [Charney \(1955\)](#) also used horizontal momentum advection to balance vorticity resulting in an additional western inertial boundary layer.

More recently, [Minobe et al. \(2017\)](#) addressed western boundary (coastal) SL for the Munk- or Stommel-type solution with vertical sidewalls and found an equatorward displacement and attenuation in coastal SL relative to the interior SL. Their relationship depends on the meridional integral of mass anomalies in the ocean interior, thus building on the idea that mass input into the boundary layer is transmitted equatorward ([Godfrey 1975](#); [Marshall and Johnson 2013](#)). This relationship allows coastal SL at a chosen latitude to be given by contributions of coastal SL at some poleward latitude and the interior SL between the two latitudes. Notably, their relationship also describes coastal SL as being independent of the details of friction. A missing element, however, in this special vertical sidewall case, is the influence of continental shelves and slopes, potentially important given the variable bathymetry along the North American east coast ([Pratt 1968](#)).

[Csanady \(1978\)](#) looked at the effect of a linearly sloping bathymetry in a steady f -plane barotropic model and showed that alongshore pressure gradients prescribed at the edge of the shelf resulted in the same gradient being present at the coast, beyond some initial insulated region. [Wang \(1982\)](#) and [Huthnance \(1987\)](#) later showed that including a continental slope increased the insulation to thousands of kilometers in scale, and in a more complex model employing stratification [Huthnance \(2004\)](#) found results similar to the barotropic case. For the case of modeling large-scale SL along western boundaries, however, allowing the Coriolis parameter to change and maintaining consistency when applying the boundary condition with the deep ocean are, as will be seen, crucial. This added complexity has contributed to limiting the study of SL in western boundary regions over sloping bathymetry. One notable result comes from [Salmon \(1998\)](#) in his study of linear ocean circulation where sloping bathymetry was described as “advecting” pressure along isobaths and the β effect (due to variable Coriolis parameter)

“advecting” pressure westward. In referring to “advection” Salmon extended an advection–diffusion analogy that had first been made by [Welander \(1968\)](#), and later [Becker and Salmon \(1997\)](#), regarding the mass transport streamfunction. Although Salmon’s model included both bathymetry and stratification, the assumption of linearity in the equation for density advection resulted in a somewhat artificial role for diapycnal diffusivity to balance any vertical velocity.

The inclusion of bathymetry (in this paper we intend bathymetry to mean sloping bottom topography) in these models resulted in solutions depending explicitly on the bottom friction parameter. As we will show, a consequence of using a western boundary vertical sidewall is that the coastal SL solution is independent of the details of friction because geostrophic flow is always distributed over the same depth range. Indeed, [Minobe et al. \(2017\)](#) list the effects of bathymetry, alterations to the vertical mode structure, and nonlinear advection as areas to explore further. In this paper we study the first two points.

We consider SL along the east coast of North America relative to the adjacent interior SL that originates from a wind-driven double gyre corresponding to a SL depression from the subpolar gyre and elevation from the subtropical gyre. Our focus is the effect of bathymetry on coastal SL for a specified ocean interior SL; we are therefore excluding the more local response to near-coastal wind stress. See, for example, [Hong et al. \(2000\)](#), [Thompson and Mitchum \(2014\)](#), [Frederikse et al. \(2017\)](#), and [Valle-Levinson et al. \(2017\)](#) for discussions on the importance of interior ocean wind stress to coastal SL. Although the North Atlantic region provided our motivation, this idealized study would apply equally well to other ocean basins with western boundary currents.

The remainder of this paper is as follows. In [section 2](#) the result of [Minobe et al. \(2017\)](#) is derived from an angular momentum argument to explicitly highlight the importance of bathymetry on coastal SL. In [section 3](#) we formulate a model that includes bathymetry for a single-layer interior and an interior with a decoupled upper layer. In [section 4](#) the effects of the continental shelf and slope on SL are presented, and in [section 5](#) this is extended to a simple stratified case. [Section 6](#) summarizes and highlights implications.

2. Vertical sidewall special case

[Minobe et al. \(2017\)](#) found a relationship between interior SL and coastal SL, for the case of an ocean with vertical sidewalls and linear dynamics. Defining η_w as the coastal (western) SL and η_i as the interior SL near the western boundary, but to the east of any western boundary current, their relationship [Eq. (14) in their paper] in the steady state can be written as

$$\left(\frac{\eta_w}{f}\right)_y = -\frac{\beta}{f^2}\eta_i, \tag{1}$$

where x and y are the zonal and meridional coordinates, respectively, subscripts x and y denote partial differentiation, f is the Coriolis parameter, and $\beta = df/dy$ (note the equation given in their paper is the integral of this with respect to y , multiplied by f).

This can be interpreted as the interior SL at each latitude contributing to a step up in coastal SL toward the south, at that latitude, which then decays to zero at the equator in a manner proportional to the sine of latitude. The effect of this at the coast is to smooth and reduce the interior signal and shift it toward the equator.

In this special case, the solution can be found without specifying the form of the friction in detail. In fact, all that is needed for the derivation are the assumptions of no normal flow at the western boundary and that friction acts in a western boundary layer. A simpler argument can be made that leads to the same conclusion.

If the active layer has constant thickness H and an applied zonal wind stress τ^x , then a simple angular momentum balance tells us that the zonally integrated wind stress must be balanced by the east–west pressure difference on vertical sidewalls (the Coriolis force integrates out because, in the steady state, as much water must flow to the north across each latitude as flows to the south). The boundary pressure perturbation p_w is related to boundary SL η_w by hydrostatic balance: $p_w = \rho g \eta_w$, with a similar relationship at the east, so the steady-state zonally integrated zonal momentum balance between the western and eastern coasts, x_w and x_e , respectively, gives

$$-\rho g H \eta_w = \int_{x_w}^{x_e} \tau^x dx, \tag{2}$$

where we have assumed that the eastern boundary SL is a constant and taken it to be zero.

Consistency with the relationship of [Minobe et al. \(2017\)](#) can be shown by noting that, for this configuration, the interior flow is determined by Sverdrup balance. For illustration purposes we will assume a purely zonal wind stress τ^x (the relationship holds for more general wind stress and a matching eastern boundary SL profile, but the derivation becomes rather more involved). In this case, Sverdrup balance is

$$-\frac{\beta v H \rho}{f} = \left(\frac{\tau^x}{f}\right)_y, \tag{3}$$

together with geostrophic balance $v = g \eta_x / f$. Integrating gives

$$\frac{\beta \rho g H}{f^2} \eta_i = \left(\int_{x_w}^{x_e} \frac{\tau^x}{f} dx\right)_y, \tag{4}$$

and then substitution of the zonal momentum balance [Eq. (2)] into the integrated Sverdrup balance [Eq. (4)] gives Eq. (1), the steady-state form of the relation found by [Minobe et al. \(2017\)](#).

The simpler determination of the western boundary SL, from Eq. (2), illustrates straightforwardly the critical nature of the assumption of vertical sidewalls. The net force on the western boundary is determined by the combination of the SL η_w and the depth range H over which the resulting pressure anomaly acts. With a bathymetric slope at the boundary, this will come to depend crucially on where currents flow. A western boundary current flowing higher up the continental slope will produce a larger SL signal for the same total transport, as the associated boundary pressure signal becomes concentrated in a shallower region, reducing the effective value of H . Recirculating currents on the slope can complicate things even further. Note that although we have found a simpler way to derive the [Minobe et al. \(2017\)](#) result, this relies on certain assumptions about interior ocean dynamics, for example, that there is no interaction with bathymetry within the basin to disturb Sverdrup balance and that there is no outflow along the northern boundary, which would imply a nonzero zonal integral of meridional velocity in Eq. (2). By relating coastal SL to nearby interior SL, [Minobe et al. \(2017\)](#) have sidestepped these requirements and produced a valuable result, albeit restricted to the case of a vertical sidewall at the west.

For this reason, it is our aim in this paper to investigate how the presence of a continental shelf and slope alters the relationship between interior ocean dynamics and boundary SL.

3. Model formulation

We begin by introducing the conceptual model. Consider the western boundary region and the interior basin as two separate domains where in the interior, between x_i and x_e , friction and vertical motion at the ocean bottom are assumed small such that Sverdrup balance governs SL for a specific wind stress and eastern boundary SL. For the western domain, between x_w and x_i , which includes bathymetry, SL at the eastern boundary of this region x_i can simply be specified as equal to the westernmost SL of the interior domain η_i .

A Northern Hemisphere coordinate system is oriented with x in the zonal and y in the meridional, as shown by the schematic in [Fig. 1](#). Note that though y increases in the poleward direction, a reference latitude,

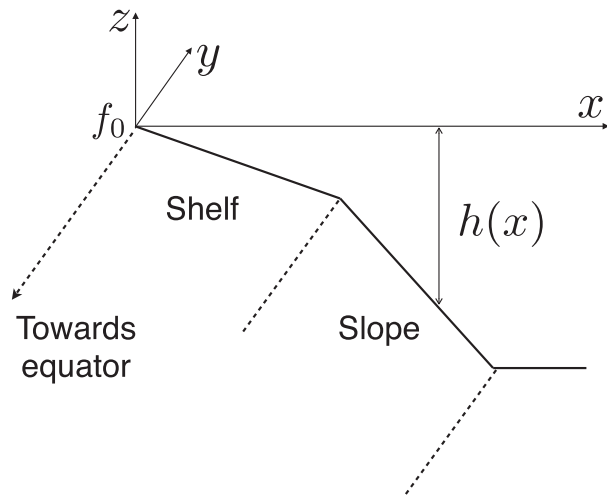


FIG. 1. Model coordinates.

$y = 0$, is set far from the equator. In the derivations that follow it is convenient to express latitude as $-y$ increasing toward the equator. Bathymetry is defined by the function $h(x)$, which tends continuously to zero at the coast ($h \rightarrow 0$ as $x \rightarrow 0$), and is taken to be uniform alongshore (i.e., independent of y).

For orientation and as an introduction to the general character of the solutions we will find, an example is shown in Fig. 2. Figure 2a shows SL contours over the combined interior and western domains for a purely zonal wind stress over the interior (producing a double gyre circulation). Figure 2b shows only the SL contours for the western domain where bathymetry is present and where there is no wind stress.

The model for the western domain begins with the steady, linearized, depth-integrated momentum and mass continuity equations:

$$f\hat{\mathbf{k}} \times h\mathbf{u} + gh\nabla\eta = \frac{\boldsymbol{\tau}}{\rho}, \quad \text{and} \quad (5)$$

$$\nabla \cdot (h\mathbf{u}) = 0, \quad (6)$$

where we define the Coriolis parameter $f = f_0 + \beta y$, density ρ , velocity \mathbf{u} , gravity g , inverse barometer corrected SL η , horizontal differential operator ∇ , and stress $\boldsymbol{\tau} = \boldsymbol{\tau}_s - \boldsymbol{\tau}_b$ with subscript s for surface stress and b for bottom friction.

Dividing Eq. (5) by f and then taking the projection of the curl in the z coordinate $\hat{\mathbf{k}} \cdot \nabla \times$ gives

$$\nabla \cdot (h\mathbf{u}) + g\nabla \times \frac{h}{f}\nabla\eta = \nabla \times \left(\frac{\boldsymbol{\tau}}{\rho f} \right), \quad (7)$$

which, by making use of the continuity equation to remove the first term on the left and the identity

$\nabla \times a\nabla q \equiv \nabla a \times \nabla q \equiv -\mathbf{J}(q, a)$ to rewrite the second term on the left, can be expressed as

$$-\mathbf{J}\left(\eta, \frac{h}{f}\right) = \nabla \times \left(\frac{\boldsymbol{\tau}}{f\rho g} \right). \quad (8)$$

Equation (8) is a form of potential vorticity equation [see (Hughes 2008) for discussion], and \mathbf{J} is known as the Jacobian operator. If now we invoke a linear friction relation for the bottom stress, giving $\boldsymbol{\tau}_b = \rho r\mathbf{u}_g$ with r the friction parameter and $\mathbf{u}_g = (g/f)\hat{\mathbf{k}} \times \nabla\eta$ the geostrophic horizontal velocity, we can expand Eq. (8) as

$$\nabla \cdot \left(\frac{r\nabla\eta}{f^2} \right) - \mathbf{J}\left(\eta, \frac{h}{f}\right) = \nabla \times \left(\frac{\boldsymbol{\tau}_s}{f\rho g} \right). \quad (9)$$

Ignoring wind stress in the western region removes the term on the right of Eq. (9) and if also we neglect friction in the zonal momentum equation on the basis that the bathymetrically steered frictional boundary currents are predominantly meridional, we can simplify Eq. (9) to

$$\frac{r}{f^2}\eta_{xx} - \left(\frac{h}{f}\right)_y\eta_x + \left(\frac{h}{f}\right)_x\eta_y = 0. \quad (10)$$

Note that while we assume that the western coastline runs meridionally, the results do generalize to the case where the coastline is at an angle ϕ to the meridional. As shown in the appendix of Minobe et al. (2017), a transformation to bathymetry following coordinates [i.e., $y = Y \cos(\phi) + X \sin(\phi)$] allows us to continue neglecting cross-shore friction. A tilted coastline would increase the alongshore pathlength for a given change in f , so we would expect the main result of such a change to be similar to a latitude-dependent friction coefficient.

Equation (10) requires boundary conditions at the coast $x = 0$, along the interface with the interior $x = x_i$, and along the northern boundary $y = 0$. The choice of x_i plays a subtle but important role in how we define the vertical structure of the ocean interior. For example, if we take the geometry considered by Stommel with a flat-bottomed basin and vertical sidewall along the western boundary, then bottom friction acts on the single-layered ocean and produces a boundary layer of thickness $\delta_s = r/(H\beta)$ (Stommel 1948) along the vertical sidewall running between the north and south. Outside (east of) this boundary layer, the flow is governed by Sverdrup balance. In this situation the interface boundary condition at x_i must be farther from the coast than the width of the boundary layer; that is, $x_i \gg \delta_s$, or $x_i = n\delta_s$ for some large n . If the vertical sidewall is replaced with sloping bathymetry of cross-shore width $L^{(x)}$, we require the interface boundary condition to be located farther from the foot of the slope than the width

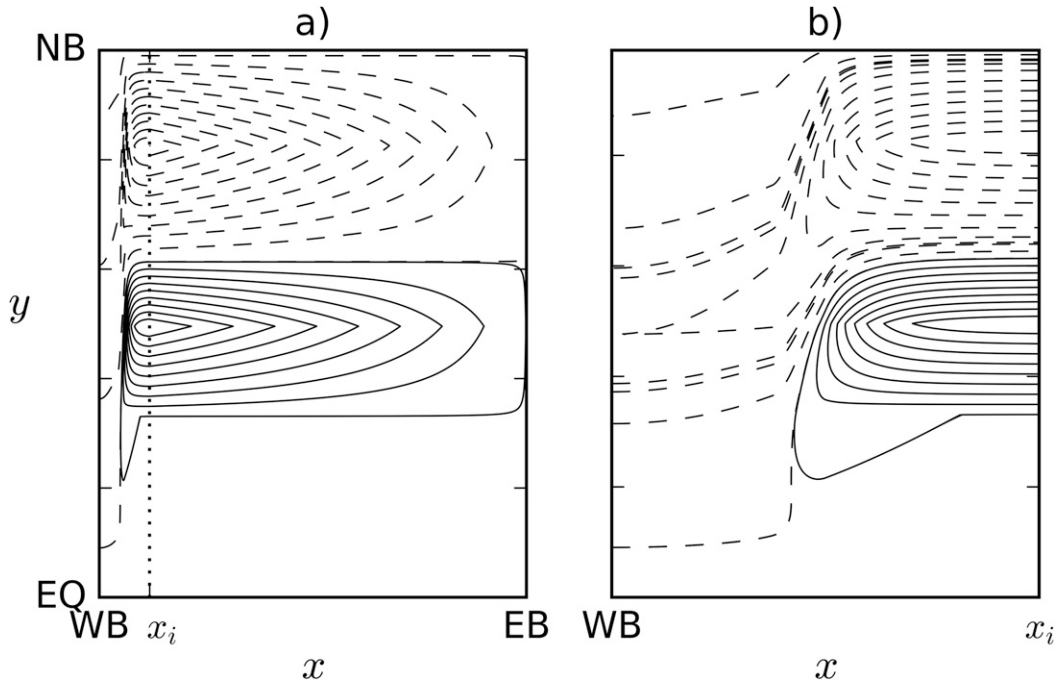


FIG. 2. Illustrative SL contours arising from a classic wind-driven double gyre for a single-layer ocean basin. (a) The whole domain. (b) Only the western region. NB, WB, and EB denote the northern ($y = 0$), western, and eastern boundaries, respectively, and EQ is the Equator ($y = -1$). Walls are assumed along the boundaries, except the western boundary, where a continental slope and shelf allow the depth to tend to zero. The dashed line x_i separates the flat-bottomed interior ocean domain (from x_i to EB) from the variable-depth western domain (from WB to x_i). Wind stress $\tau = [\tau^x(y), 0]$ acts in the interior only, with Sverdrup balance assumed. Solid and dashed contours denote positive and negative sea level anomalies, respectively. For comparison with later results $P_a = 5$, $S = 0.75$, and $H_s = 0.075$ (these parameters are defined later).

of the boundary layer; that is, $x_i = L^{(x)} + n\delta_s$. The schematic in Fig. 3a shows a cross section of the western domain for this scenario, with H the maximum ocean depth.

Consider now taking $n = 0$, so that the interface boundary condition is along the foot of the slope. In such a situation we are effectively specifying a boundary layer width of zero, which implies that bottom friction does not act east of the foot of the slope. This can be thought of as specifying the interior ocean as having an upper layer of uniform thickness H , which makes contact with the bathymetry at a distance $L^{(x)}$ from the coast, and a motionless bottom layer, which plays no part in the western domain. The schematic in Fig. 3b shows a cross section of the western domain for this scenario. This boundary condition approach is consistent with that used by Csanady (1978) and for our application has the advantage, ostensibly, of allowing the model to capture the effects of basic stratification at sloping bathymetry for an ocean in which most of the flow is confined to the surface layers. Note, however, that this configuration leads to a subtle issue with

boundary conditions (discussed later) that can produce difficulties.

We now have two different modeling scenarios. In the single-layer case (Fig. 3a), the boundary condition is $\eta = \eta_i$ at $x = L^{(x)} + n\delta_s$, which allows space for a frictional boundary layer to the east of the continental slope. In the upper-layer case (Fig. 3b) we have $\eta = \eta_i$ at $x = L^{(x)}$ (i.e., $n = 0$), as there is no viscosity acting to the east of the topography in the active layer. In both cases, $\eta = 0$ at $y = 0$ (i.e., inactivity to the north). Along the coast we have no normal flow, $uh = 0$; however, with depth tending to zero at the coast, from Eq. (5) we obtain τ tending to zero at the coast, that is, a balance between wind and bottom stress. Since we neglect wind stress in the western region, this means bottom stress νr is zero, and hence (since ν is zero and in geostrophic balance), $\eta_x = 0$ at $x = 0$.

To better understand the behavior of Eq. (10), it is nondimensionalized, along with the boundary conditions, with the following scales:

$$\eta = \Phi\eta^*, h = Hh^*, x = L^{(x)}x^*, y = L^{(y)}y^*, \quad (11)$$

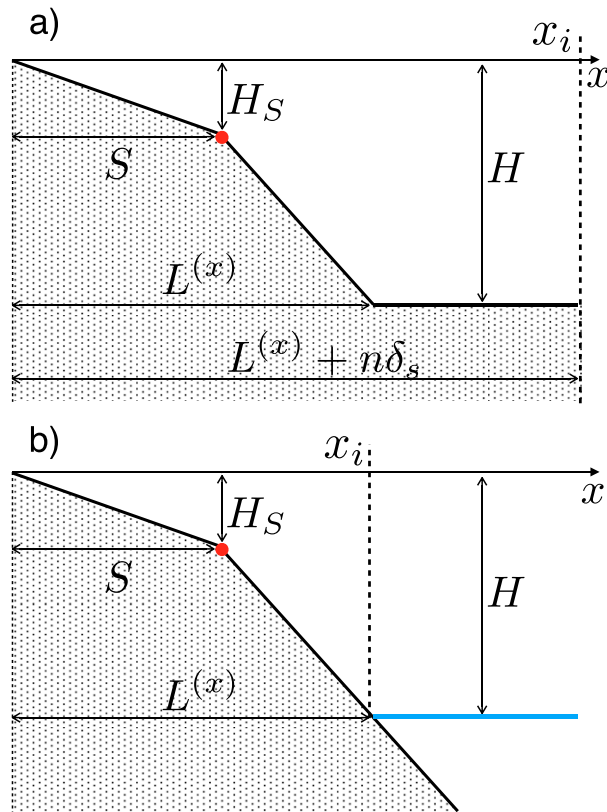


FIG. 3. Across-slope section of bathymetry: (a) homogeneous single-layer ocean of depth H with $n \gg 1$ and interior boundary located at $x_i = L^{(x)} + n\delta_s$. (b) Upper-layer ocean of thickness H with $n = 0$ with interior boundary located at $x_i = L^{(x)}$. The red dot denotes the shelf break, where S is the relative width of the shelf and H_S is the relative depth of the shelf break. Throughout this paper S and H_S are normalized by $L^{(x)}$ and H , respectively.

where $*$ denotes nondimensional variables, Φ is the maximum magnitude of the SL along the boundary with the interior ocean η_i , and the alongshore length scale is given by $L^{(y)} = f_0/\beta$. In the alongshore direction the domain is $-1 < y^* \leq 0$, where $y^* = -1$ is the equator. The nondimensional variables η^* and h^* are of order unity, and the interior boundary is at $x_i^* = 1 + n\delta_s/L^{(x)}$, where $x_i^* = 1$ is the foot of the continental slope.

Until now the derivation has been consistent with bathymetry that changes both along- and cross-shore; that is, $h = h(x, y)$. We now assume uniformity alongshore, expand the derivatives of $h(x)/f(y)$, and substitute Eqs. (11) into Eq. (10) to give

$$\left[\frac{r}{(L^{(x)}f_0)^2} \right] \frac{1}{(1+y^*)^2} \eta_{xx}^* + \left(\frac{H\beta}{L^{(x)}f_0^2} \right) \frac{h^*}{(1+y^*)^2} \eta_x^* + \left(\frac{H\beta}{L^{(x)}f_0^2} \right) \frac{h_x^*}{1+y^*} \eta_y^* = 0. \quad (12)$$

Dividing through by the coefficient of the first term then gives the final form of the equations, nondimensionally, as

$$\eta_{xx} + P_a h(x) \eta_x + P_a h_x(x)(1+y) \eta_y = 0, \quad (13)$$

$$\eta_x = 0 \quad \text{at} \quad x = 0, \quad (14)$$

$$\eta = \eta_i(y) \quad \text{at} \quad x = x_i = 1 + \frac{n}{P_a}, \quad \text{and} \quad (15)$$

$$\eta = 0 \quad \text{at} \quad y = 0, \quad (16)$$

where the $*$ notation has been dropped, and P_a is a nondimensional parameter given by $P_a = \beta H L^{(x)}/r$. We discuss this parameter in detail below, but to describe how it appears in the boundary condition [Eq. (15)], we first note its relation to the width of the Stommel boundary layer. Defining the boundary layer width as $\delta_s = r/(H\beta)$ (Stommel 1948), we obtain $P_a = L^{(x)}/\delta_s$; that is, P_a is the combined width of shelf and slope divided by the Stommel width. The cross-shore nondimensional domain width can then be written as $1 + n/P_a$.

To interpret the meaning of the parameter P_a , it is useful to introduce a streamfunction gh/f for a fictitious velocity field:

$$U = \left(\frac{gh}{f} \right)_y, \quad V = - \left(\frac{gh}{f} \right)_x, \quad (17)$$

equivalent to $(U, V) = \nabla(gh/f) \times \hat{\mathbf{k}}$, which, in flat regions, is simply a westward flow at the long Rossby wave speed.¹ Equation (9) can then be written as an analog advection–diffusion equation:

$$-\nabla \cdot (\kappa \nabla \eta) + \mathbf{U} \cdot \nabla \eta = \mathbf{S}, \quad (18)$$

with the “diffusion coefficient” defined as $\kappa = gr/f^2$ and the source term by $\mathbf{S} = -\nabla \times (\boldsymbol{\tau}_s/f\rho)$. Here we interpret SL η to be “advected” tangentially to the streamlines of gh/f (quotation marks denote analogous diffusion and advection, as opposed to actual advection by the current). This implies that SL is rapidly “advected” alongshore over steep bathymetry and with an increasing rapidity cross-shore at lower latitudes, where we also note that the diffusion coefficient becomes large. Figure 4 shows the contours of gh/f in a western boundary region with bathymetry, along which SL is “advected” toward a single point at the meeting of equator and zero depth. Note that SL will always be “advected” toward this point and therefore “diffusion” (friction) is necessary for coastal SL

¹Note added in proof: this “advection” velocity was described earlier by Tyler and Käse (2000).

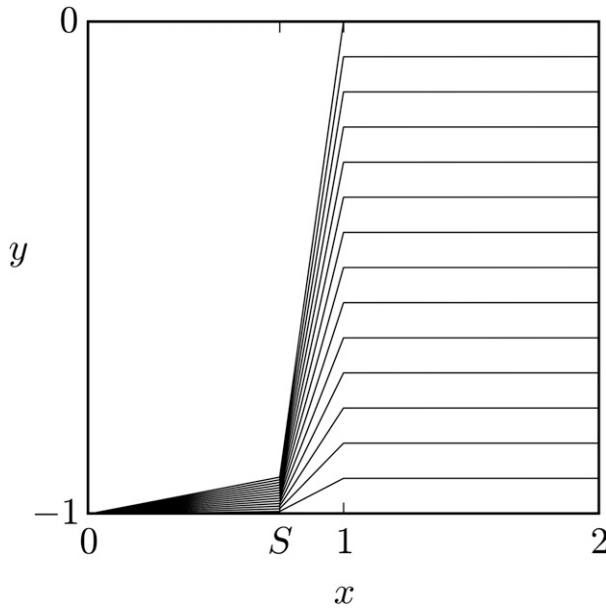


FIG. 4. Contours of $gh(x)f(y)$ for relative shelf width $S = 0.75$ and relative shelfbreak depth $H_S = 0.075$. Nondimensional across- and alongshore coordinates are given by x and y , respectively.

to be influenced by the interior SL. The nonlinear dependence of SL on f (decreasing f allows SL contours to cross isobaths) indicates why constant f -plane models would suggest greater bathymetric insulation between coast and interior; that is, constant f does not allow the effectiveness of bathymetry to steer SL to change with latitude. Note that, although we are using a beta plane in order to simplify the geometry as far as possible, Eq. (9) and the advection–diffusion analogy hold exactly on a sphere, so there will be no qualitative difference in the more general case, although the insulating effect of topography will increase at higher latitudes as β reduces.

In the context of thermal fluids, a nondimensional Péclet number (Pe) is often defined as a measure of the relative importance of advection and diffusion with respect to unidirectional thermal energy transport; Pe greater than unity implies advection is dominant and Pe less than unity that diffusion is dominant. In our analogy we have defined an analogous “Péclet number” P_a as a measure of the relative importance of cross-shore “advection” and “diffusion” with respect to the transport of SL. Note that we do not have an alongshore “Péclet number” due to the omission of zonal friction that implicitly assumes that alongshore ‘advection’ dominates alongshore “diffusion.”

In terms of coastal SL, the purely “advective” part of SL transport is invariant to scale (following gh/f contours). Increasing the importance of cross-shore “diffusion,” therefore, by decreasing P_a should result in a

coastal SL signal that more closely resembles interior SL. In other words, increasing friction r and/or decreasing the scales of the bathymetry (H and $L^{(x)}$) should increase interior SL penetration to the coast. Since $P_a = L^{(x)}/\delta_s$, this also implies that decreasing the cross-shore scale of the shelf and slope relative to the Stommel boundary layer width increases SL penetration.

It is important to note that the parameter P_a does not account for the variable coefficients in Eq. (13). This means that locally, at any given (x, y) , “advection” and “diffusion” (and therefore SL penetration) depend on the geometry of the bathymetry $h(x)$ and latitude y .

As will be demonstrated in the next section, the theory suggests two independent controls on the contribution of interior SL to coastal SL: first through the parameter P_a , grouping together the effect of overall bathymetric scale and the friction parameter; and second the definition of the function $h(x)$ independent of scale, that is, the relative proportions of the continental shelf and slope.

4. Coastal SL parameter study

In this section we present solutions of the advection–diffusion Eqs. (13)–(16). Section 4a looks at the effect of the “Péclet number” P_a without changing the relative proportions of the bathymetry for the single layer model (Fig. 3a), where $x_i = 1 + n/P_a$. Section 4b repeats this investigation for the upper-layer model (Fig. 3b), where $x_i = 1$. Section 4c then looks at the effect of bathymetric configuration by changing the relative width and depth scales of the shelf and slope.

In the following we are concerned only with the western domain, taking the SL along the interior boundary $\eta_i(y)$ as a given function. For this we assume that wind stress drives subpolar and subtropical gyres in the interior and that along the western edge of the interior at $x_i = 1 + n/P_a$ there is zero net zonal transport. From geostrophic balance this gives the following condition:

$$\int_{Yf} \frac{1}{Yf} \frac{d\eta_i}{dy} dy = 0, \tag{19}$$

where Y is the latitudinal extent of the domain.

A piecewise linear function is used for η_i with coefficients chosen to satisfy Eq. (19). A buffer region of constant SL is used for some distance north of the equator (see black curve in Fig. 6 below).

Bathymetry is defined by a piecewise linear function in x on the basis that it gives the simplest yet most illustrative means of studying the effects of including a continental shelf and slope. In Figs. 3a and 3b we

define two extra parameters: depth at the shelf break H_S and shelf width S . We take these parameters as nondimensional ($0 \leq H_S \leq 1$ and $0 \leq S \leq 1$) with scales H and $L^{(x)}$, respectively.

The bathymetry is therefore defined by

$$h(x) = \begin{cases} \alpha_1 x, & \text{for } 0 \leq x \leq S, \\ \alpha_1 S + \alpha_2(x - S), & \text{for } S < x \leq 1, \\ 1, & \text{for } 1 < x \leq 1 + n/P_a, \end{cases} \quad (20)$$

where

$$\alpha_1 = \frac{H_S}{S} \quad \text{and} \quad (21)$$

$$\alpha_2 = \frac{1 - H_S}{1 - S} \quad (22)$$

are the nondimensionalized shelf and slope gradients. In sections 4a and 4b the bathymetric configuration is fixed with $H_S = 0.075$ and $S = 0.75$, which, if we assume an illustrative depth $H = 2000$ m and cross-shore width $L^{(x)} = 130$ km, gives a shelf and slope with drops of 150 and 1850 m, respectively, and widths of 97.5 and 32.5 km, respectively. The characteristics of the shelf and slope along the east coast of North America vary considerably, but this configuration captures the basic structure.

Before looking at the dependence of SL on P_a , it is useful to establish a characteristic value for P_a based on $H = 2000$ m, $L^{(x)} = 130$ km, $f_0 = 10^{-4} \text{ s}^{-1}$, $\beta = 1.667 \times 10^{-11} \text{ (m s)}^{-1}$, and some value of the friction parameter r , which can be considered as a linear approximation of quadratic friction (Gill 1982). Two values for r used in the literature, $r = 0.0005 \text{ m s}^{-1}$ (Chapman and Brink 1987; Xu and Oey 2011) and $r = 0.001 \text{ m s}^{-1}$ (Csanady 1978; Huthnance 2004), give an illustrative parameter value for P_a as 8.67 and 4.33, respectively.

Equations (13) to (16) will now be solved using a Crank–Nicholson finite-difference scheme with non-dimensional resolution $\Delta x = 0.003$ and $\Delta y = 0.00063$, which was found to give resolution independence. We also apply a slight bathymetric gradient over flat-bottomed portions of bathymetry for numerical purposes, though it is small enough to be insignificant in terms of the solution.

a. Sea level dependence on P_a —Single layer

In this subsection we use the Stommel-type model (Fig. 3a), where $x_i = 1 + n/P_a$ and H is the depth scale of the ocean. We take $n \geq 7$ to be large enough that the frictional boundary layer has decayed west of the interior boundary.

Figure 5 gives SL in the western domain for three values of $P_a = \beta H L^{(x)}/r$: 0.1, 10, and 200, where 0.1 is small and 200 large relative to the illustrative characteristic values, which are between 4.3 and 8.7. By comparing Figs. 5a, 5c, and 5d we see that the frictional “boundary layer” extends farther offshore when P_a is small, relating to either a large frictional parameter or small-scale bathymetry, demonstrating why the cross-shore domain width is dependent on P_a (incorporating δ_s). The solutions in Figs. 5b–d also show that smaller values of P_a result in greater penetration of the interior SL to the coast; that is to say, between the interior and the coast, the SL depression and elevation experience less equatorward displacement and less attenuation when P_a is smaller.

From our advection–diffusion analogy, Fig. 5d ($P_a = 200$) relates to a highly “advective” solution where SL contours follow gh/f streamlines closely, resulting in significant equatorward displacement and attenuation of the interior SL. Figure 5c ($P_a = 10$) relates to a relatively “advective” solution, and there is less displacement and attenuation of SL. Finally, Figs. 5a and 5b ($P_a = 0.1$) show a relatively “diffusive” solution with SL experiencing less displacement and attenuation. As suggested by the analogy, increasing the friction parameter and/or decreasing the scale of the overall shelf and slope increases penetration. The implication is that SL within the western domain is sensitive to the representation of bottom friction when continental shelves and slopes are included into the model. Furthermore, it shows that the depth and width scales of the overall bathymetry alter coastal SL, so resolving the continental slope can be important.

Focusing on coastal SL $\eta(x = 0, y)$, Fig. 6a shows interior and coastal SL for $P_a = 0.1, 1, 10,$ and 100 . The coastal SL in each case can be described as a smoothed version of the interior SL with an equatorward displacement and an attenuation that in general increases with displacement; both increase as P_a increases. A comparison of the depression minimum for $P_a = 0.1$ and $P_a = 10$ shows the magnitude reduces by nearly 35% and the alongshore displacement increases by approximately 1600 km (in the case where $\beta = 1.667 \times 10^{-11}$ and $f_0 = 10^{-4} \text{ s}^{-1}$). Increasing the friction parameter, and/or decreasing the scale of the combined shelf and slope, increases the penetration of SL to the coast.

The displaced and attenuated SL depression shown in Fig. 6a supports the result presented by Higginson et al. (2015) where the interior ocean SL tilt (the transition from SL depression to elevation where the Gulf Stream heads offshore) is observed at the coast displaced equatorward by 10° of latitude and attenuated from 1 m to 20 cm. The result here suggests that equatorward displacement of the tilt would be reduced in the

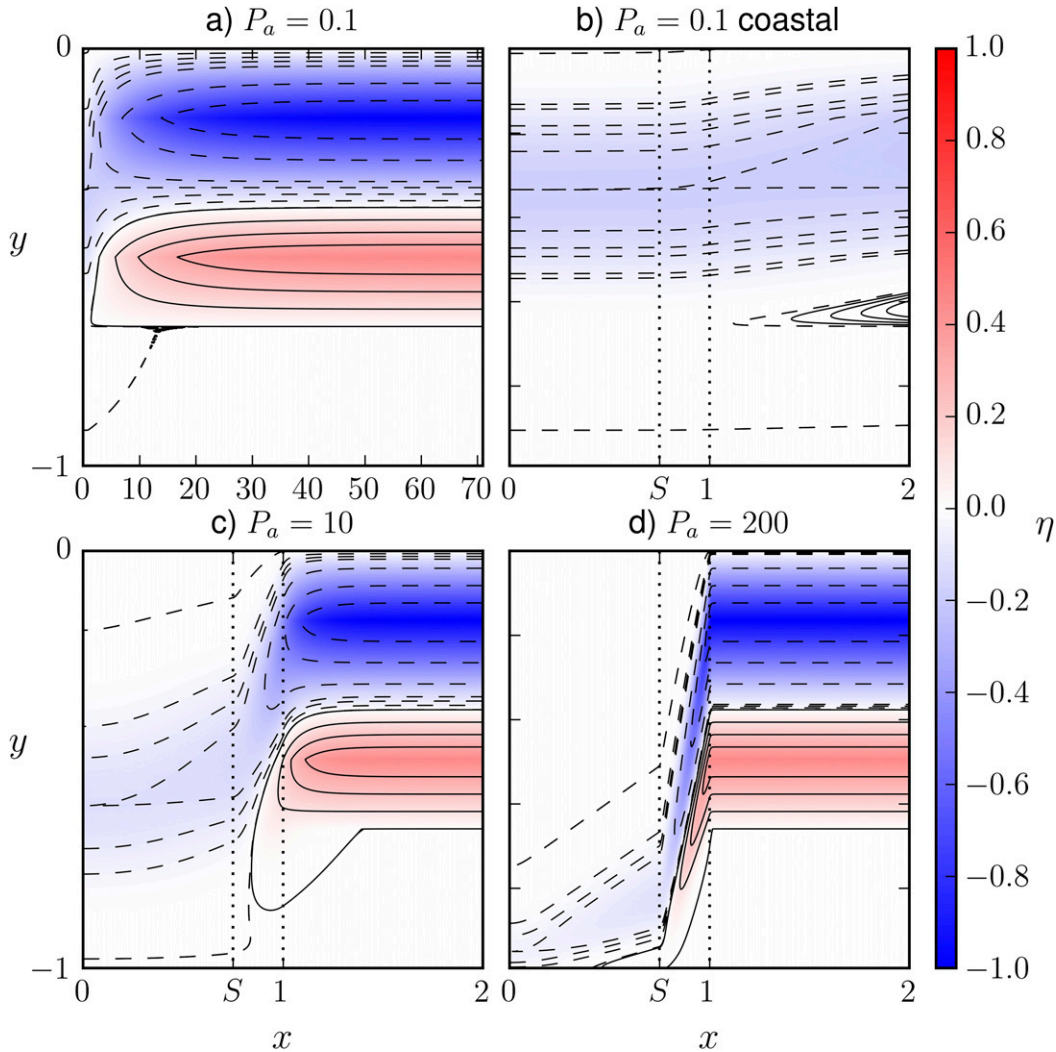


FIG. 5. Western domain sea level contours $\eta(x, y)$ (nondimensional; dashed negative) for relative shelf width $S = 0.75$ and relative shelfbreak depth $H_S = 0.075$, where x and y are the nondimensional across- and alongshore coordinates, respectively. Vertical dotted lines indicate the shelf break at $x = S$ and slope floor at $x = 1$. (a) $P_a = 0.1$, (b) $P_a = 0.1$ coastal close up, (c) $P_a = 10$, and (d) $P_a = 200$.

following circumstances: 1) the combined width of the shelf and slope are reduced, 2) the depth to the foot of the slope is reduced, and 3) bottom drag is increased. The same is implied for the magnitude of the tilt. Note that while [Higginson et al. \(2015\)](#) do not comment on overall bathymetric scale, they do speculate that the width of the continental shelf [i.e., the definition of $h(x)$] plays a role in the latitudinal position of the coastal SL tilt, an issue we cover in [section 4c](#).

An important result can be demonstrated by looking at the limit $P_a \rightarrow 0$. This can be interpreted as either the high friction limit or the narrow topography (vertical sidewall) limit ($L^{(v)} \rightarrow 0$). In [Fig. 6a](#) we see that, for low P_a , the solution approaches the friction-independent

vertical sidewall solution of [Minobe et al. \(2017\)](#). Thus, for a single-layer model, the vertical sidewall represents the maximum possible penetration of the interior SL.

b. Sea level dependence on P_a —Upper layer ($n = 0$)

In this subsection we model an upper layer of the ocean ([Fig. 3b](#)) where $x_i = 1$ and H is the scale for the thickness of the upper layer.

The general behavior of SL in this case is qualitatively similar to the single-layer case, and the “advection–diffusion” analysis of the previous subsection holds. There is, however, a distinct quantitative difference in coastal SL. In [Fig. 6b](#), the solid lines show coastal SL for $P_a = 0.1, 1, 10$, and 100 (this is the upper-layer counterpart

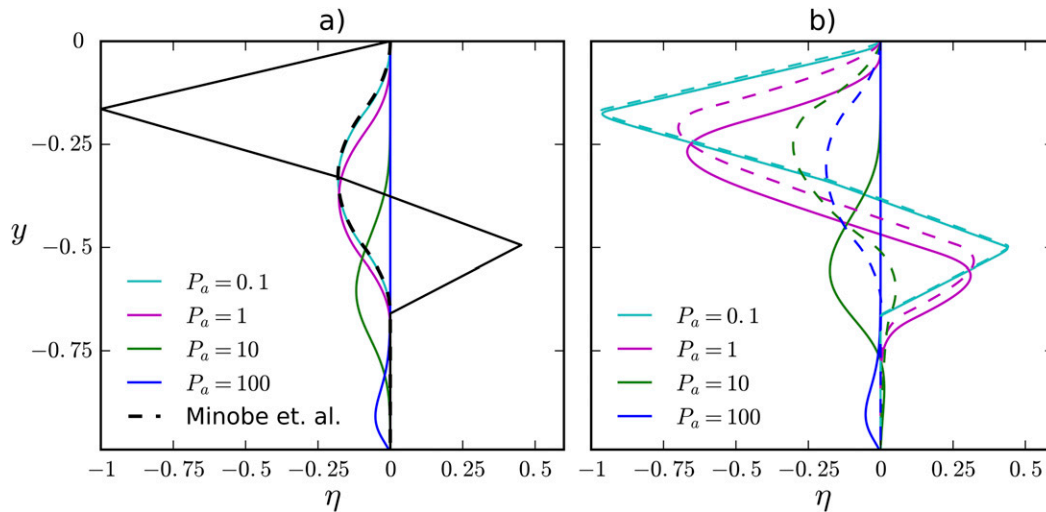


FIG. 6. Coastal sea level, $\eta(y)$ (nondimensional), for $P_a = [0.1, 1, 10, 100]$ with interior sea level, $\eta_i(y)$ (solid black line), where y is the nondimensional alongshore coordinate (equator at $y = -1$). The relative shelf width is $S = 0.75$ and the relative shelf break depth is $H_s = 0.075$. (a) For a single-layer homogeneous interior, the black dashed line is the coastal sea level for the case of a vertical sidewall using Minobe et al.’s (2017) Eq. (14) with our interior sea level η_i . (b) Solid lines are coastal sea level $\eta(y)$ for the interior ocean with an active upper layer and motionless lower layer using $\eta_i(y)$ (solid black line) at the interior boundary. Dashed lines are the associated vertical sidewall solution [Minobe et al. 2017, their Eq. (14)] when using the true interior sea level [Eq. (25)].

to the single-layer version; Fig. 6a), and it is clear that displacement and attenuation of the interior SL is reduced. This is particularly noticeable for $P_a < 10$, where the coastal SL begins to closely resemble interior SL.

This result suggests that, consistent with the results of Csanady (1978), it is possible to have greater penetration of interior ocean SL than the vertical sidewall limit permits. However, there is a subtlety that is being missed in this case: the “interior” SL should be imposed on the ocean side of the boundary where bottom friction is zero, but in using Eq. (10) we are effectively imposing a value on the slope side of that boundary.

The subtlety and importance of how the boundary between the interior ocean and western region is defined can be demonstrated by allowing the bottom friction parameter to decrease as we move away from the coast. Defining friction as $R = R(x)$ requires Eq. (10) to be rewritten as

$$\frac{(R\eta_x)_x}{f^2} - \left(\frac{h}{f}\right)_y \eta_x + \left(\frac{h}{f}\right)_x \eta_y = 0. \tag{23}$$

We take R to be continuous, constant over the shelf and slope (between $x = 0$ and $x = L^{(x)}$), and decreasing to zero between $x = L^{(x)}$ and x_i ; that is,

$$R = \begin{cases} r, & \text{if } x < L^{(x)}, \\ rG(x), & \text{if } x \geq L^{(x)}, \end{cases} \tag{24}$$

where $G(x) = 1$ at $x = L^{(x)}$ and $G(x) = 0$ at $x = x_i$ (x_i is a point at which the frictional boundary layer has decayed).

The extent to which the frictional boundary layer extends offshore now depends on how $G(x)$ is defined, specifically, where we choose x_i to be [$G(x_i) = 0$ implies geostrophic balance in the depth integrated zonal flow]. Moving x_i closer to the slope therefore decreases the width of the frictional boundary layer.

Integrating Eq. (23) from $L^{(x)}$ to x_i (a region in which h is constant), and recalling that $\delta_s = r/H\beta$, gives

$$\eta_i = \eta_{L^{(x)}} + \delta_s (\eta_x)_{L^{(x)}}, \tag{25}$$

where subscript $L^{(x)}$ denotes evaluation at $x = L^{(x)}$. This relation leads to a surprising result. Equation (25) shows that SL on the shelf and slope is independent of the details of offshore friction (east of $L^{(x)}$). We can infer this by noting that if we assume that SL at the edge of the slope $\eta_{L^{(x)}}$ is known, then SL on the shelf and slope can be found by solving Eq. (10) with $\eta_{L^{(x)}}$ as the boundary SL. We can then obtain η_i from Eq. (25) without any knowledge of $G(x)$. Surprisingly, therefore, this result shows that the details of offshore friction are only important in determining the width of the frictional boundary layer, not SL on the shelf and slope.

This result becomes relevant to the upper-layer model, used in this section, if we take the limit of $x_i \rightarrow L^{(x)}$; that is, we take x_i to be infinitesimally close to the edge of the slope at $L^{(x)}$. To denote this we will use a subscript $-$ to represent the shoreward point and subscript $+$ to represent the offshore point. Across these points, the friction

parameter drops to zero, so that $R_- = r$ and $R_+ = 0$. Equation (23) now becomes

$$\eta_+ = \eta_- + \delta_s(\eta_x)_-. \quad (26)$$

This relation shows that despite the distance between η_+ and η_- being infinitesimally small, SL in the ocean interior η_+ is not the same as that on the shoreward side of the boundary η_- . The upper-layer model (Fig. 3b) therefore fails to specify the true ocean interior SL that is being used in the single-layer model (Fig. 3a). The degree to which it fails is proportional to δ_s (inversely proportional to P_a), and the result is a jump in SL between western and interior domains, calculated by projecting the slope $(\eta_x)_-$ out to a distance of one Stommel width beyond the boundary.

The jump in SL is required to conserve depth-integrated mass flux. A discontinuity in bottom stress implies a discontinuity in offshore Ekman flux, which therefore implies a discontinuity in the onshore geostrophic flow, and hence a jump in SL. This is also a problem with section 10 of Csanady (1978). In that paper the coastal influence of a linear meridional SL slope is considered with the conclusion that the entire amplitude of the slope penetrates to the coast. There is, however, no way to connect this solution to a frictionless ocean interior, without invoking a step in sea level.

The upper-layer model appears to allow greater penetration of the interior SL signal because it is effectively using a larger-amplitude interior SL signal. In fact the upper- and single-layer models are the same, except that the upper-layer model implicitly uses a larger-amplitude interior SL. To demonstrate this point, the dashed lines in Fig. 6b show the coastal SL for the case with a vertical sidewall when the equivalent interior SL, calculated from Eq. (25) or (26), is used. The dashed curves show that the vertical sidewall solutions remain the limit of penetration as in Fig. 6a.

c. Coastal SL and bathymetric configuration

In reality continental shelves and slopes have varied proportions (configurations), and so we look now at the dependence of SL on $h(x)$, that is, the scales of the shelf and slope relative to each other and independent of P_a .

Changing the relative proportions of the shelf and slope requires the location of the shelf break to change without changing the combined depth and width of the shelf and slope. This simply means keeping P_a fixed and allowing the shelfbreak parameters H_S and S to vary between zero and one. For example, by increasing H_S from 0.075 to 0.5 the depth scale of the shelf is increased by $(0.5 - 0.075)H$ and that of the slope is decreased by the same amount.

So far we have looked at the penetration of interior SL at the coast for specific values of P_a , S , and H_S . In the remainder of this section we explore the parameter space of these three parameters more thoroughly, using the single-layer model (Fig. 3a) exclusively.

In the following we focus on a single reference point of the coastal SL signal to investigate attenuation and displacement. For this we choose the coastal SL minimum and define it as η_{\min} . We are therefore interested in the attenuation of η_{\min} and the displacement of η_{\min} as shown in Figs. 7a and 7b. Note that the displacement is measured relative to $y = 0$, whereas the open ocean SL minimum is at $y = -1/6$, meaning that displacements smaller than 0.167 would actually be northward relative to the open ocean SL (though no such displacements occur).

In Figs. 7c and 7d we plot attenuation and displacement of η_{\min} as a function of H_S (the shelfbreak depth relative to the maximum depth H) and P_a with the shelf width S held constant. We use $0.01 \leq H_S \leq 0.99$, $1 \leq P_a \leq 50$, and $S = 0.75$. In Figs. 7e and 7f we plot attenuation and displacement of η_{\min} as a function of S (the shelf width relative to the combined width of shelf and slope $L^{(x)}$) and P_a with the shelfbreak depth H_S held constant. We use $0.05 \leq S \leq 0.95$, $1 \leq P_a \leq 50$, and $H_S = 0.075$. In Figs. 7c–f lighter colors denote greater attenuation and displacement (less penetration).

Figures 7c and 7d show that displacement and attenuation are maximized in the approximate region $0.2 < H_S < 0.7$. As H_S becomes small or large relative to this region, displacement and attenuation decrease. This suggests that geometries where the shelf is quite shallow increase penetration. This appears to hold for the range of P_a considered.

Figures 7e and 7f show that for $P_a < 20$, attenuation and displacement decrease as S increases, that is, as the shelf becomes wider. For $P_a > 20$, smaller values of S also decrease attenuation and displacement.

As a whole, the results of Fig. 7 show that penetration of interior SL to the coast increases rapidly (nonlinearly) as P_a decreases and that this holds for any configuration of shelf and slope. Surprisingly, however, the results also show that wide shallow shelves increase the penetration of interior SL to the coast. More generally, the results show that configurations tending toward vertical wall-like geometries have increased penetration. Therefore, while it is true that broader combined shelf and slope $L^{(x)}$ in comparison to the Stommel boundary layer width (i.e., larger P_a) leads to greater insulation of the coast from the deep ocean, a broader, shallower shelf region for a given overall width has the opposite effect.

The strong dependence of the solution on geometry and scale raises the question of the effect of model resolution on coastal SL; for example, a 1° ocean model has

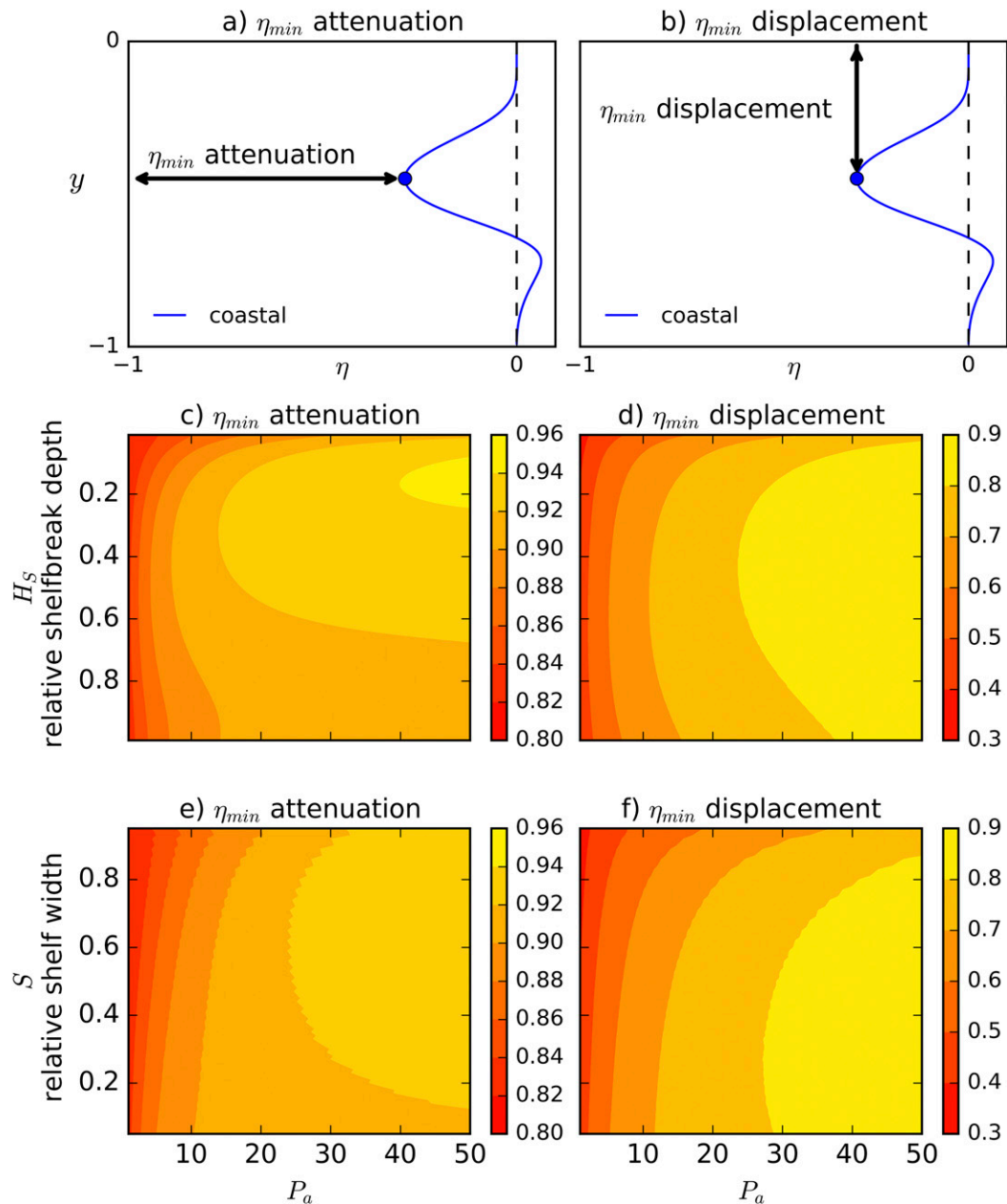


FIG. 7. Shown are (a) how the attenuation of the coastal sea level minimum η_{\min} is measured for (c) and (e), and (b) how the displacement of the coastal SL minimum η_{\min} is measured for (d) and (f). In (a) and (b) the blue curve represents the nondimensional coastal sea level $\eta(y)$. (c) Color map of attenuation of η_{\min} as a function of shelfbreak depth H_S and P_a with $S = 0.75$. (d) Color map of the displacement of η_{\min} as a function of shelfbreak depth H_S and P_a with $S = 0.75$. (e) Color map of the attenuation of η_{\min} as a function of shelf width S and P_a with $H_S = 0.075$. (f) Color map of the displacement of η_{\min} as a function of shelf width S and P_a with $H_S = 0.075$. In (c)–(f) lighter colors denote greater attenuation and displacement (less penetration).

perhaps only one or two grid points on the combined shelf and slope. Assuming, for example, $P_a = 5$ with a cross-shore width of $L^{(x)} = 130$ km, a shelf width of 97.5 km, and a slope width of 32.5 km, we found that a cross-shore resolution of 9 km (three grid points on the slope) resulted in close to a 15% decrease in the

magnitude of the coastal minimum compared to the high-resolution converged solution. In this illustrative example we found six grid points on the slope (5.2-km resolution) gave a coastal minimum that deviated from the high-resolution solution by only 1% in magnitude. This indicates that ocean models with a resolution that is

coarse compared to the width of the shelf and slope could be distorting coastal SL owing to a poor representation of bathymetry.

It is clear that the solutions do depend on the geometry of the shelf and slope, as well as the overall scales and the friction parameter; in the next section we extend the model by considering a 1.5-layer interior. The following analysis will use dimensional quantities.

5. Dimensional model with 1.5 layers

It is more realistic to assume background stratification will alter the vertical mode structure and change how the flow interacts with bathymetry. In this section we create a simple stratified model by allowing the upper-layer depth along the interior boundary to be non-uniform; that is, $H = H(y)$.

In contrast to the previous sections, we now directly calculate SL and upper-layer thickness in the whole interior for a specified interior-only wind stress using a reduced gravity model with a single active upper layer of constant thickness h_e along the eastern boundary x_e . For this we use a density difference between the two layers of 1.02 kg m^{-3} and apply a zonal wind stress that varies meridionally:

$$\tau^x(y) = \begin{cases} \tau_0 \left[1 - \cos\left(\frac{3\pi y}{L^{(y)}}\right) \right], & \text{for } -\frac{2}{3}L^{(y)} < y \leq 0, \\ 0, & \text{for } -L^{(y)} < y \leq -\frac{2}{3}L^{(y)}, \end{cases} \quad (27)$$

where τ_0 (N m^{-2}) is the amplitude (see Fig. 8 for the wind stress profile). The interior domain is of width 4500 km with constant top-layer depth at the eastern boundary of $h_e = 900$ m.

We then take SL along the westernmost edge of the reduced-gravity interior model and use it as the interior boundary condition for the western domain η_i (as in previous sections).

For the western domain, we represent an upper-layer thickness that changes with latitude by allowing the depth h in the model developed in section 3 to vary alongshore; that is, $h = h(x, y)$. The depth h is defined by projecting the upper-layer thickness at the interior boundary, which changes in y , up to the slope. The effect of this change on the theory developed in section 3 is that the path along which SL is “advected” changes to reflect the modified gh/f contours. From Eq. (17) we now have a fictitious advecting zonal velocity $U = gh_y/f - gh\beta/f^2$, where the first term is new.

We consider two different cases. In the first case we allow only a slight latitudinal variability in the thermocline thickness. This relates to weak interior gyres (solid

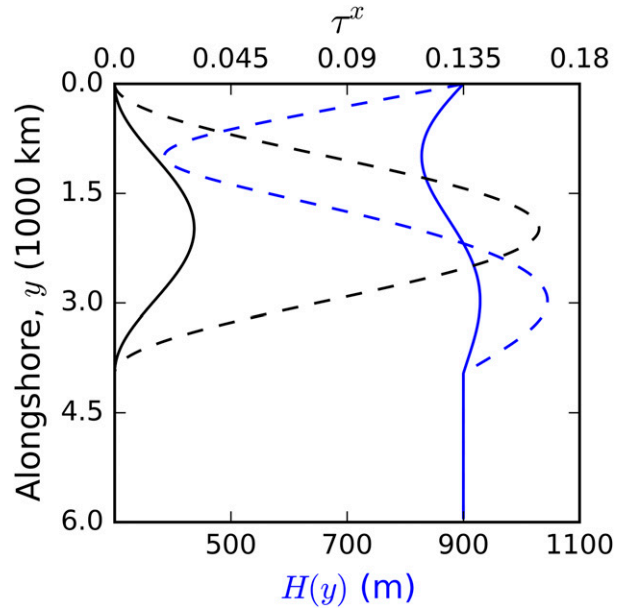


FIG. 8. Solid lines are wind stress (black) and resulting upper-layer thickness (blue) along the interior boundary x_i for $\tau_0 = 0.015 \text{ N m}^{-2}$. Dashed lines are wind stress (black) and resulting upper-layer thickness (blue) along the interior boundary x_i for $\tau_0 = 0.082 \text{ N m}^{-2}$. Here $y = 0$ is the poleward reference point where $f_0 = 10^{-4}$. The reduced gravity interior has a width of 4500 km, and the eastern boundary upper layer thickness is $h_e = 900$ m.

lines in Fig. 8). In the second case we allow a larger latitudinal variation in the upper-layer thickness. This relates to stronger interior gyres (dashed lines in Fig. 8). In the latter case, we note that because of the larger latitudinal variation of h , there is a reversal in the direction of U , the zonal “advecting” velocity, in the northern part of the subpolar gyre. This results in a somewhat artificial frictional boundary layer extending to the northeastern corner (not shown).

Figure 9a shows the interior boundary SL, the new coastal SL, and the vertical wall solution for the weak interior gyre case. We show in addition the corresponding solution for the single-layer model with P_a adjusted for a comparative thickness. The figure shows that slight variability in the upper-layer thickness allows for a slight change in the distribution of the coastal SL (the attenuation is slightly smaller). Figure 9b repeats Fig. 9a for the stronger gyre case. Now we clearly see increased penetration (decreased attenuation) beyond the vertical wall limit.

Vertical mode interaction allows the thickness of the upper layer to be redistributed such that it decreases over a poleward portion of the interior. This decrease enables the interior SL over this poleward portion to penetrate farther toward the coast before making contact with the bathymetry; this can increase penetration

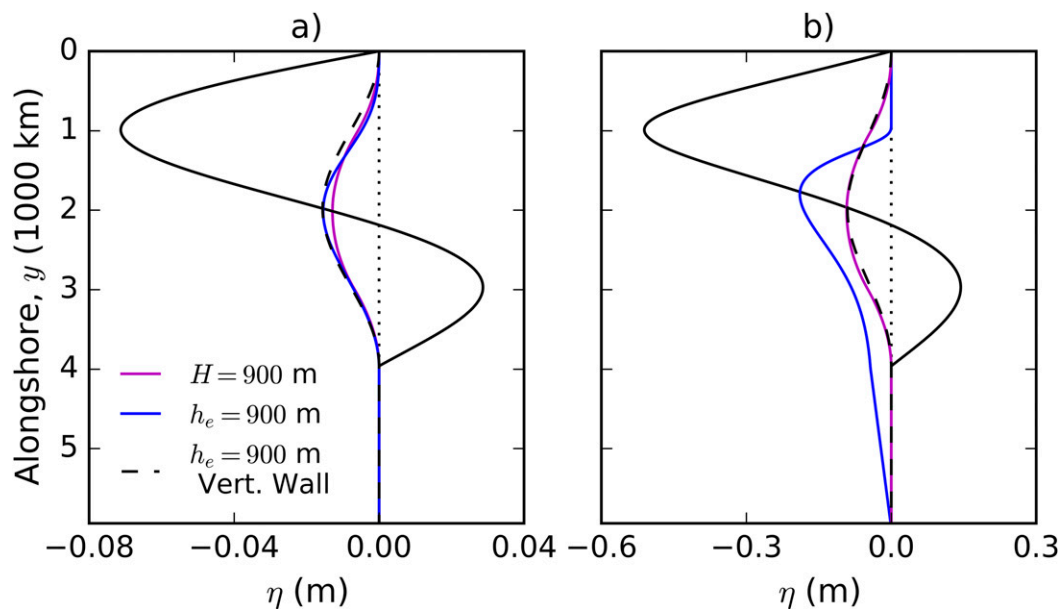


FIG. 9. Interior and coastal sea level using a variable thickness upper layer for two wind stress magnitudes: (a) $\tau_0 = 0.015 \text{ N m}^{-2}$ and (b) $\tau_0 = 0.082 \text{ N m}^{-2}$ (see Fig. 8 wind stress and layer thickness profiles). For both (a) and (b) the black solid curve is interior sea level η_i , the solid blue line is the resulting coastal sea level, the dashed black line is the resulting 1.5-layer vertical wall coastal sea level, and the magenta line is the coastal sea level using the single-layer model with a comparable interior sea level. For the nonvertical wall coastal sea levels (blue and magenta) we use a shelf width of 97.5 km, a shelfbreak depth of 150 m, eastern boundary thickness $h_e = 900 \text{ m}$, $r = 0.0166 \text{ m s}^{-1}$, $H = 900 \text{ m}$, and $L^{(x)} = 113.3 \text{ km}$ (equivalent $P_a = 0.1$).

of the subpolar SL depression. On the other hand, the upper layer thickens toward the equator suggesting a decrease in penetration of the subtropical SL elevation. In effect our “Péclet number” is changing with latitude, smallest where the upper-layer thickness is thinnest. The reversal of the characteristic direction in the strong gyre case means the validity of this solution is questionable. This raises questions about SL penetration when a linear approximation may not be appropriate for modeling thermocline depth. We leave this investigation for future studies.

6. Discussion and conclusions

We have shown that the assumption of a vertical sidewall at the coast within a western boundary allows coastal SL to be independent of layer thickness and the friction parameter and that the vertical sidewall solution is a special limit case for the more general problem that includes sloping bathymetry.

A β -plane theory has been developed for a general bathymetry that is uniform alongshore showing that interior SL transmits to the coast analogously to the steady “advection–diffusion” of a thermal fluid. For an interior SL originating from a wind-driven double gyre, corresponding to a coastal SL depression from the

subpolar gyre and elevation from the subtropical gyre, the theory demonstrates that ocean interior sea level can penetrate to the coast having been attenuated and displaced equatorward. The analogy describes SL as being “advected” along gh/f contours with sloping bathymetry steering (“advecting”) SL contours along isobaths and the β effect steering (“advecting”) contours westward. For bathymetry that tends to zero at the coast and Coriolis parameter that vanishes at the equator, the interior SL does not register at the coast in the limit of no friction (though technically a friction stress is required at the singularity at the coastal equator point). The addition of alongshore friction, however, introduces cross-shore “diffusion” and allows SL contours to cross gh/f contours such that the interior SL penetrates to the coast, where greater penetration implies less equatorward displacement and attenuation of the depression and elevation signal.

A nondimensional “Péclet number” ($P_a = HL^{(x)}\beta/r = L^{(x)}/\delta_s$, where δ_s is the Stommel boundary layer thickness), quantifying the relative importance of “advection” and “diffusion,” is defined to demonstrate how smaller combined shelf-slope width and depth scales and a larger friction parameter increase “diffusion” relative to “advection” and increase SL penetration. Increasing the scale of the combined bathymetry and

decreasing the friction parameter have the opposite effect. Using this parameter it has been demonstrated that for a single-layer interior, increasing the friction parameter toward infinity ($P_a \rightarrow 0$) results in coastal SL tending toward the vertical sidewall solution for any bathymetry, implying that the vertical sidewall is the maximum penetration limit for a single-layered interior. Since $P_a = L^{(x)}/\delta_s$ is the width of the combined shelf and slope divided by the width of the Stommel boundary layer δ_s , we find that open ocean influence on coastal SL is essentially the same as the vertical sidewall case only in regions where the combined shelf and slope width lie within the Stommel boundary layer; that is, P_a is small.

A distinction is drawn between a single-layer interior and an interior with a decoupled upper layer of uniform thickness that makes contact with the continental slope at a distance $L^{(x)}$ from the coast. In the former the frictional boundary layer extends into the deep ocean, but in the latter it is restricted to the shelf and slope region. After noting a subtlety in the boundary condition for this case we find it to be exactly the same as the single-layer case, but with the possibility of smaller layer thickness, which results in greater SL penetration. The model is then extended to the case where upper and lower interior layers interact, producing an upper-layer thickness that is nonuniform alongshore and thinner where SL is depressed due to the subpolar gyre. It is shown that this can enhance penetration further, by reducing the steering effect of the continental slope on the poleward SL contours. This can be thought of as the parameter P_a changing meridionally (smaller where the upper layer is thinner).

Independently of the overall scales accounted for in P_a , it is shown that the configuration of shelf and slope can significantly alter how interior SL transmits to the coast. For realistic overall scales giving $P_a \leq 10$, it is found that wider and shallower shelves, relative to the overall scales, maximize SL penetration. This raises questions about the effect of model resolution on coastal SL, and in our experiments it was found that fewer than six grid points on the slope (~ 5 -km resolution for a 30-km slope) could produce noticeable error in the coastal SL. Further questions arise, and remain to be investigated, when the stratification leads to characteristics that propagate information away from the western boundary.

The results and analysis presented here have implications for our understanding of the drivers of coastal SL. Higginson et al. (2015) showed that the 1-m difference in interior SL across the location where the Gulf Stream moves into deep water is represented at the coast by an attenuated and equatorward displaced version. They noted that this was not explained by f -plane theoretical models, which suggest that oceanic SL features should not penetrate to the coast over the observed

alongshore distance. The β -plane model developed here explains why a displaced and attenuated tilt in coastal SL should be expected and that, for example, an increased interior SL due to a weakened subpolar gyre (decreased tilt) would affect the coast.

Higginson et al. (2015) also suggested that the position of the coastal tilt might be explained by the narrow shelf at the Florida Straits. This study has shown that topography that is well approximated by a vertical wall ($L^{(x)} \ll \delta_s$) should enable greater penetration of the interior signal. More generally, moving northward of 32°N along the North American east coast, the combined shelf and slope width decreases significantly, and this would suggest a transition to reduced bathymetric insulation. This is important for predictions of coastal SL if we consider that the tilt of interior SL experiences latitudinal variability driven by the North Atlantic Oscillation (NAO) (McCarthy et al. 2015). If the insulating properties of the shelf and slope change meridionally, then a northward shift in the interior SL tilt would not necessarily result in a coastal SL tilt shifted by the same distance. This may also have implications for the suggestion that the latitudinal positions of SL-rise hot spots along the eastern United States are being determined by the NAO (Valle-Levinson et al. 2017).

The results and analysis presented here suggest that how bathymetry is configured and how finely it is resolved, in addition to the representation of bottom friction, are potentially quite important to ocean models focusing on SL in western boundaries. While the linear model used here has been intentionally simple, many additions can be made, notably the impact of including momentum advection and including time dependence to explore shorter-time-scale SL adjustments in a more sophisticated numerical model.

Acknowledgments. We thank the reviewers for helping to improve this manuscript with their suggestions. This work was supported by the Natural Environment Research Council (Anthony Wise: NE/L002469/1), (Chris W. Hughes: NE/K012789/1), and (Jeff A. Polton: NE/L003325/1).

REFERENCES

- Becker, J. M., and R. Salmon, 1997: Eddy formation on a continental slope. *J. Mar. Res.*, **55**, 181–200, <https://doi.org/10.1357/0022240973224418>.
- Chapman, D. C., and K. H. Brink, 1987: Shelf and slope circulation induced by fluctuating offshore forcing. *J. Geophys. Res.*, **92**, 11 741–11 759, <https://doi.org/10.1029/JC092iC11p11741>.
- Charney, J. G., 1955: The Gulf Stream as an inertial boundary layer. *Proc. Natl. Acad. Sci. USA*, **41**, 731–740, <https://doi.org/10.1073/pnas.41.10.731>.

- Csanady, G. T., 1978: The arrested topographic wave. *J. Phys. Oceanogr.*, **8**, 47–62, [https://doi.org/10.1175/1520-0485\(1978\)008<0047:TATW>2.0.CO;2](https://doi.org/10.1175/1520-0485(1978)008<0047:TATW>2.0.CO;2).
- Frederikse, T., S. Karen, K. A. Caroline, and R. Riccardo, 2017: The sea-level budget along the northwest Atlantic coast: GIA, mass changes, and large-scale ocean dynamics. *J. Geophys. Res. Oceans*, **122**, 5486–5501, <https://doi.org/10.1002/2017JC012699>.
- Gill, A. E., 1982: *Atmosphere-Ocean Dynamics*. Academic Press, 662 pp.
- Godfrey, J., 1975: On ocean spin-down I: A linear experiment. *J. Phys. Oceanogr.*, **5**, 399–409, [https://doi.org/10.1175/1520-0485\(1975\)005<0399:OOSIAL>2.0.CO;2](https://doi.org/10.1175/1520-0485(1975)005<0399:OOSIAL>2.0.CO;2).
- Higginson, S., K. R. Thompson, P. L. Woodworth, and C. W. Hughes, 2015: The tilt of mean sea level along the east coast of North America. *Geophys. Res. Lett.*, **42**, 1471–1479, <https://doi.org/10.1002/2015GL063186>.
- Hong, B., W. Sturges, and A. J. Clarke, 2000: Sea level on the U.S. East Coast: Decadal variability caused by open ocean wind-curl forcing. *J. Phys. Oceanogr.*, **30**, 2088–2098, [https://doi.org/10.1175/1520-0485\(2000\)030<2088:SLOTUS>2.0.CO;2](https://doi.org/10.1175/1520-0485(2000)030<2088:SLOTUS>2.0.CO;2).
- Hughes, C. W., 2008: A form of potential vorticity equation for depth-integrated flow with a free surface. *J. Phys. Oceanogr.*, **38**, 1131–1136, <https://doi.org/10.1175/2007JPO3809.1>.
- Huthnance, J., 1987: Along-shelf evolution and sea levels across the continental slope. *Cont. Shelf Res.*, **7**, 957–974, [https://doi.org/10.1016/0278-4343\(87\)90008-2](https://doi.org/10.1016/0278-4343(87)90008-2).
- , 2004: Ocean-to-shelf signal transmission: A parameter study. *J. Geophys. Res.*, **109**, C12029, <https://doi.org/10.1029/2004JC002358>.
- Lin, H., K. R. Thompson, J. Huang, and M. Véronneau, 2015: Tilt of mean sea level along the Pacific coasts of North America and Japan. *J. Geophys. Res. Oceans*, **120**, 6815–6828, <https://doi.org/10.1002/2015JC010920>.
- Marshall, D. P., and H. L. Johnson, 2013: Propagation of meridional circulation anomalies along western and eastern boundaries. *J. Phys. Oceanogr.*, **43**, 2699–2717, <https://doi.org/10.1175/JPO-D-13-0134.1>.
- McCarthy, G. D., I. D. Haigh, J. J.-M. Hirschi, J. P. Grist, and D. A. Smeed, 2015: Ocean impact on decadal Atlantic climate variability revealed by sea-level observations. *Nature*, **521**, 508–510, <https://doi.org/10.1038/nature14491>.
- Minobe, S., M. Terada, B. Qiu, and N. Schneider, 2017: Western boundary sea level: A theory, rule of thumb, and application to climate models. *J. Phys. Oceanogr.*, **47**, 957–977, <https://doi.org/10.1175/JPO-D-16-0144.1>.
- Munk, W. H., 1950: On the wind-driven ocean circulation. *J. Meteor.*, **7**, 80–93, [https://doi.org/10.1175/1520-0469\(1950\)007<0080:OTWDOC>2.0.CO;2](https://doi.org/10.1175/1520-0469(1950)007<0080:OTWDOC>2.0.CO;2).
- Pratt, R. M., 1968: Atlantic continental shelf and slope of the United States: Physiography and sediments of the deep-sea basin. U.S. Department of the Interior Geological Survey Professional Paper 529-B, 50 pp., <https://pubs.usgs.gov/pp/0529b/report.pdf>.
- Sallenger, A. H., Jr., K. S. Doran, and P. A. Howd, 2012: Hotspot of accelerated sea-level rise on the Atlantic coast of North America. *Nat. Climate Change*, **2**, 884–888, <https://doi.org/10.1038/nclimate1597>.
- Salmon, R., 1998: Linear ocean circulation theory with realistic bathymetry. *J. Mar. Res.*, **56**, 833–884, <https://doi.org/10.1357/002224098321667396>.
- Stommel, H., 1948: The westward intensification of wind-driven ocean currents. *Eos, Trans. Amer. Geophys. Union*, **29**, 202–206, <https://doi.org/10.1029/TR029i002p00202>.
- Thompson, P., and G. Mitchum, 2014: Coherent sea level variability on the North Atlantic western boundary. *J. Geophys. Res. Oceans*, **119**, 5676–5689, <https://doi.org/10.1002/2014JC009999>.
- Tyler, R. H., and R. Käse, 2000: A ‘string function’ for describing the propagation of large-scale potential energy anomalies in a rotating fluid. *Geophys. Astrophys. Fluid Dyn.*, **92**, 31–64, <https://doi.org/10.1080/03091920008203710>.
- Valle-Levinson, A., A. Dutton, and J. B. Martin, 2017: Spatial and temporal variability of sea level rise hot spots over the eastern United States. *Geophys. Res. Lett.*, **44**, 7876–7882, <https://doi.org/10.1002/2017GL073926>.
- Wang, D.-P., 1982: Effects of continental slope on the mean shelf circulation. *J. Phys. Oceanogr.*, **12**, 1524–1526, [https://doi.org/10.1175/1520-0485\(1982\)012<1524:EOCSOT>2.0.CO;2](https://doi.org/10.1175/1520-0485(1982)012<1524:EOCSOT>2.0.CO;2).
- Welander, P., 1968: Wind-driven circulation in one- and two-layer oceans of variable depth. *Tellus*, **20A**, 1–16, <https://doi.org/10.1111/j.2153-3490.1968.tb00347.x>.
- Woodworth, P. L., C. W. Hughes, R. J. Bingham, and T. Gruber, 2012: Towards worldwide height system unification using ocean information. *J. Geod. Sci.*, **2**, 302–318, <https://doi.org/10.2478/v10156-012-0004-8>.
- Xu, F.-H., and L.-Y. Oey, 2011: The origin of along-shelf pressure gradient in the Middle Atlantic Bight. *J. Phys. Oceanogr.*, **41**, 1720–1740, <https://doi.org/10.1175/2011JPO4589.1>.